



Article

Assessing Thallium Elemental Systematics and Isotope Ratio Variations in Porphyry Ore Systems: A Case Study of the Bingham Canyon District

Angus Fitzpayne ^{1,2,*} , Julie Prytulak ^{1,3} , Jamie J. Wilkinson ^{1,4,5}, David R. Cooke ^{5,6}, Michael J. Baker ^{5,6} and Clara C. Wilkinson ^{4,5}

¹ Department of Earth Science and Engineering, Imperial College London, Exhibition Road, London SW7 2AZ, UK; julie.prytulak@durham.ac.uk (J.P.); j.wilkinson@nhm.ac.uk (J.J.W.)

² School of Earth Sciences, The University of Melbourne, Parkville, Melbourne, Victoria 3010, Australia

³ Department of Earth Sciences, University of Durham, DH1 3LE, UK

⁴ London Centre for Ore Deposits and Exploration (LODE), Department of Earth Sciences, Natural History Museum, Cromwell Road, London SW7 5BD, UK; clara.c.wilkinson@gmail.com

⁵ ARC Centre of Excellence in Ore Deposits (CODES), University of Tasmania, Hobart, Tasmania 7001, Australia; d.cooke@utas.edu.au (D.R.C.); michael.baker@utas.edu.au (M.J.B.)

⁶ Transforming the Mining Value Chain (TMVC), an Australian Research Council (ARC) Industrial Transformation Research Hub, University of Tasmania, Hobart, Tasmania 7001, Australia

* Correspondence afitzpayne@student.unimelb.edu.au

Received: 1 October 2018; Accepted: 19 November 2018; Published: 26 November 2018



Abstract: The Bingham Canyon porphyry deposit is one of the world's largest Cu-Mo-Au resources. Elevated concentrations of thallium (Tl) compared to average continental crust have been found in some brecciated and igneous samples in this area, which likely result from mobilization of Tl by relatively low temperature hydrothermal fluids. The Tl-enrichment at Bingham Canyon therefore provides an opportunity to investigate if Tl isotope ratios reflect hydrothermal enrichment and whether there are systematic Tl isotope fractionations that could provide an exploration tool. We present a reconnaissance study of nineteen samples spanning a range of lithologies from the Bingham district which were analysed for their Tl content and Tl isotope ratios, reported as parts per ten thousand ($\epsilon^{205}\text{Tl}$) relative to the NIST SRM997 international standard. The range of $\epsilon^{205}\text{Tl}$ reported in this study (-16.4 to $+7.2$) is the largest observed in a hydrothermal ore deposit to date. Unbrecciated samples collected relatively proximal to the Bingham Canyon porphyry system have $\epsilon^{205}\text{Tl}$ of -4.2 to $+0.9$, similar to observations in a previous study of porphyry deposits. This relatively narrow range suggests that high-temperature ($>300^\circ\text{C}$) hydrothermal alteration does not result in significant Tl isotope fractionation. However, two samples $\sim 3\text{--}4$ km away from Bingham Canyon have higher $\epsilon^{205}\text{Tl}$ values ($+1.3$ and $+7.2$), and samples from more distal (~ 7 km) disseminated gold deposits at Melco and Barney's Canyon display an even wider range in $\epsilon^{205}\text{Tl}$ (-16.4 to $+6.0$). The observation of large positive and negative excursions in $\epsilon^{205}\text{Tl}$ relative to the mantle value ($\epsilon^{205}\text{Tl} = -2.0 \pm 1.0$) contrasts with previous investigations of hydrothermal systems. Samples displaying the most extreme positive and negative $\epsilon^{205}\text{Tl}$ values also contain elevated concentrations of Tl-Sb-As. Furthermore, with the exception of one sample, all of the Tl isotopic anomalies occur in hydrothermal breccia samples. This suggests that $\epsilon^{205}\text{Tl}$ excursions are most extreme during the migration of low-temperature hydrothermal fluids potentially related to sediment-hosted gold mineralization. Future investigation to determine the host phase(s) for Tl in breccias displaying both chalcophile element enrichment and $\epsilon^{205}\text{Tl}$ excursions can potentially provide new information about hydrothermal fluid composition and could be used to locate sites for future porphyry exploration.

Keywords: thallium; isotope geochemistry; Bingham Canyon; porphyry Cu-Au-Mo; hydrothermal alteration

1. Introduction

1.1. Porphyry Ore Deposits

Porphyry ore deposits are large anomalies of sulfide-hosted mineralization caused by magmatic-hydrothermal processes, and constitute significant resources of Cu (~75% of the world's reserves), Mo (~50%), Au (~20%) and lesser amounts of other metals such as Ag [1]. They are associated both genetically and spatially with porphyritic intrusions in the upper crust, which cool and exsolve hydrothermal fluids containing water-soluble Cl and S species that extract metals from the source magmas and wall-rocks [2]. The fluids are focused along cracks within the host intrusion and surrounding country rock, and precipitate ore minerals due to fluid cooling and mixing, phase separation (vapor/liquid), and wall-rock reaction [3]. Although porphyry ore mineralization is centred upon the host intrusion, mineralization may occur elsewhere in the surrounding rocks due to metal transport in cooler hydrothermal fluids that form skarns, sediment-hosted mineralization, or epithermal deposits, which may be proximal or distal to the porphyry intrusions [1,4–8]. The formation of such deposits may be influenced by country rock lithology: for example, skarns require reactive, carbonate-rich rocks to form, whereas the genesis of epithermal deposits may be facilitated by permeable rocks, possibly aided by extensive fracturing and brecciation [1,2].

1.2. Bingham Canyon Cu-Mo-Au Deposit

This study focuses on the Bingham Canyon district in the USA, which contains the Bingham Canyon porphyry Cu-Au-Mo deposit. This is among the largest known porphyry Cu deposits in terms of total contained metals; for example, in 2005, Bingham Canyon was identified as the seventh largest porphyry deposit in the world in terms of contained Cu [9]. The deposit contains around 28 MT of Cu, making it a supergiant deposit [10], with an average grade of 0.88 wt.%; 0.81 MT Mo at 0.02 wt.%; and 1600 T Au at 0.5 µg/g [9]. High-grade (~10 µg/g) gold mineralization occurs in a skarn, located ~2 km to the west of the Bingham Canyon mine, and is associated with quartz and pyrite, as well as enrichment in arsenic, mercury, and thallium [11].

The Bingham Canyon mine is situated in the Oquirrh Mountains between the Basin and Range province and the Cordilleran fold-thrust belt [12,13], near Salt Lake City, Utah (Figure 1). Although most porphyry deposits are associated with compressional tectonic regimes [14], the Bingham Canyon intrusions are suggested to have formed by melting of previously metasomatized lithosphere during a phase of Eocene extension ([15,16], and references therein). The host rocks for the deposit consist of several igneous lithologies, which form the Bingham and Last Chance stocks [13,16,17]. The Bingham intrusions are intermediate to felsic in composition (57–65 wt.% SiO₂; [18]) and oxidized in nature ($fO_2 = NNO + 1.7$; [19]); the compositional range may be a result of either magmatic differentiation [15] or magma mixing [20]. The quartz monzonite porphyry (QMP) is the main “causative” intrusion and hosts a large proportion of the copper ore body [13,16]. Other porphyries occur as dikes that intruded the QMP [16] within a relatively short time period of ~0.3 My [21]. The country rocks into which the Bingham Canyon porphyries were emplaced are Pennsylvanian in age, and were folded and faulted during multiple orogenies through the Mesozoic [18,22]. They vary in composition between sandstones and limestones and their metamorphic counterparts, and locally they are mineralized [18].

Surrounding the Bingham Canyon mine are several sediment-hosted gold deposits, including the Barneys Canyon and Melco deposits located ~7 km to the north (Figure 1). Both exhibit characteristics of Carlin-type gold deposits [23], which have been linked to low temperature, magmatic-hydrothermal fluids [8,24]. The sediment-hosted gold deposits in the Bingham district have been inferred to represent

part of a distal, asymmetric Au-As alteration facies related to the Bingham Canyon deposit [23,25]. A variety of palaeothermometry techniques appear to support a genetic link between the gold deposits and the Bingham Canyon porphyry system [23,26], although it has been suggested that the Bingham Canyon system was neither hot enough nor large enough to cause such distant gold mineralization in the epithermal environment, and that a different low-temperature hydrothermal fluid was introduced, which mixed with local meteoric waters [12,27].

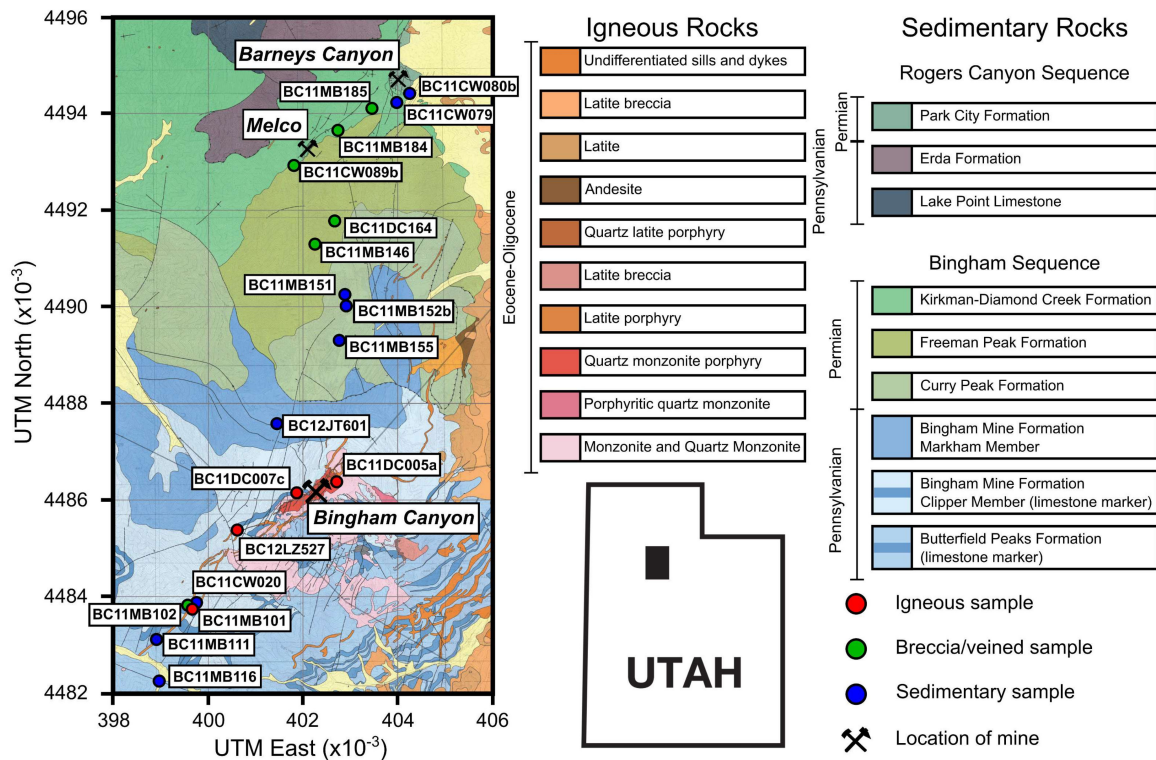


Figure 1. Geological map of the area surrounding the Bingham Canyon porphyry Cu deposit; all samples analysed for Tl isotope compositions are marked with sample name and lithology; inset map of Utah showing study area (black rectangle), modified after [23].

The Bingham Canyon deposit has been extensively studied and therefore provides a good basis for this reconnaissance study, in which a well-characterized set of samples distributed roughly N–S through the Bingham district is examined. The investigation focuses on thallium and its isotope ratios, supplemented by whole-rock geochemistry, to establish the extent of Tl isotopic fractionation in porphyry-hydrothermal systems and to evaluate its utility for tracing hydrothermal fluid flow and depositional processes. Although the investigation focuses on Bingham Canyon as a case study, the findings of this study may have wider implications for future investigations in other hydrothermal systems.

1.3. The Geochemistry of Thallium and Thallium Isotope Systematics

Thallium (Tl) is a volatile, highly incompatible trace metal, which displays both lithophile and chalcophile affinities [28–31]. Where sulfides are absent, Tl behaves like the large-ion lithophile (LIL) elements K, Rb, and Cs, due to their similar ionic radii (K^+ : 1.33 Å; Tl^+ : 1.49 Å; Rb^+ : 1.49 Å; Cs^+ : 1.65 Å; e.g., [32,33]), and preferentially partitions into K-bearing phases, such as biotite ($K_D = 8.6$) and K-feldspar ($K_D = 3.67$) [34]. Although some experimental studies have predicted that sulfides might contain high abundances of Tl [35], only a minority (14 of 38) of natural sulfides analysed in a recent study [36] contained Tl abundances above the detection limit (0.2 µg/g). This makes it likely that K-rich silicates will dominate Tl-partitioning over coexisting sulfide phases. The only relevant

Tl redox species in most natural environments is Tl^+ [37]; Tl^{3+} is thought to be present only in near surface or aqueous conditions in the laboratory [38].

Thallium has two stable isotopes, ^{203}Tl (29.5%) and ^{205}Tl (70.5%). Thallium isotope ratios are measured in parts per ten thousand (ϵ units) relative to the NIST SRM997 Tl standard, where

$$\epsilon^{205}\text{Tl} = 10^4 \times \frac{^{205}\text{Tl}/^{203}\text{Tl}_{\text{sample}} - ^{205}\text{Tl}/^{203}\text{Tl}_{\text{SRM997}}}{^{205}\text{Tl}/^{203}\text{Tl}_{\text{SRM997}}} \quad (1)$$

The primitive mantle contains an estimated 0.0035 $\mu\text{g/g}$ Tl, whereas the crust has ~ 0.5 $\mu\text{g/g}$ (see review in [31]). Thallium concentrations in low-temperature hydrothermal systems are generally higher than in high-temperature regimes (e.g., [39,40]). Both the mantle and continental crust display restricted isotope compositions of $\epsilon^{205}\text{Tl} = -2.0 \pm 1.0$ [31,41], although some natural variability is implied by the fact that this range is slightly larger than the long-term, external 2 s.d. (standard deviation) analytical reproducibility, which is conservatively estimated to be ± 0.5 epsilon units [31,42]. Magmatic processes do not appear to cause significant Tl isotope fractionations [33], allowing Tl isotopes to be applied, for example, as useful tracers of different sediment types in variably evolved arc lavas [43–46]. In general, stable isotope fractionations strongly increase in magnitude with decreasing temperature (e.g., [47]). Indeed, previous studies have highlighted the large differences in Tl isotopic behavior in low- (<150 °C) and high-temperature (300–400 °C) hydrothermal systems [39,40,48], with low-temperature alteration causing variable, isotopically light values ($\epsilon^{205}\text{Tl} = -2$ to -16), and high-temperature alteration having a limited effect on $\epsilon^{205}\text{Tl}$ [39]. The lack of response in Tl isotope signatures to both high-temperature hydrothermal and magmatic processes suggests that Tl isotope investigations in porphyry systems will be most sensitive to the relatively low-temperature hydrothermal processes that post-date, and/or are distal to, the main porphyry ore-forming event.

1.4. Thallium Isotope Studies of Hydrothermal Ore Deposits

Several previous studies have evaluated the potential of Tl isotopic measurements as tracers of hydrothermal processes in ore deposits. Baker et al. [48] focused on Tl isotope behavior in porphyry deposits, and presented Tl concentration and isotope variations in rocks from the Collahuasi Formation (Chile), which is composed of lava flows, pyroclastic rocks, and porphyritic intrusions of varying composition, emplaced between 240 and 300 Ma [49]. These older igneous rocks displayed varying degrees of alteration, caused by younger porphyry ore-related intrusions (~ 35 Ma; [50]), some of which were also analysed by Baker et al. [48]. The assorted samples from the Collahuasi district contained 0.1–3.2 $\mu\text{g/g}$ Tl, and Tl was found to preferentially partition into K-bearing phases. Abundances of Tl and K were interpreted to be governed by hydrothermal, and not magmatic, processes. Thallium isotope compositions varied between -5.1 and $+0.1$ $\epsilon^{205}\text{Tl}$ (Figure 2), with a mean value (-2.0 ± 2.0 ; 2 s.d.) that is indistinguishable from the mantle value [31,41]. The igneous and hydrothermal processes within the Collahuasi Formation therefore appear not to have caused significant Tl isotope fractionation. No systematic relationship between $\epsilon^{205}\text{Tl}$ and whole-rock concentration of K_2O (enriched in the potassic-altered core of porphyry systems) or Cu was found, leading to the suggestion that Tl isotopes could not be used as a tracer for mineralization in porphyry systems.

However, the study of Baker et al. [48] was limited to samples that were mostly altered at temperatures of 300–400 °C [51]. Consequently, it is perhaps unsurprising that the $\epsilon^{205}\text{Tl}$ values measured showed neither systematic variation nor significant deviations from the mantle range (Figure 2).

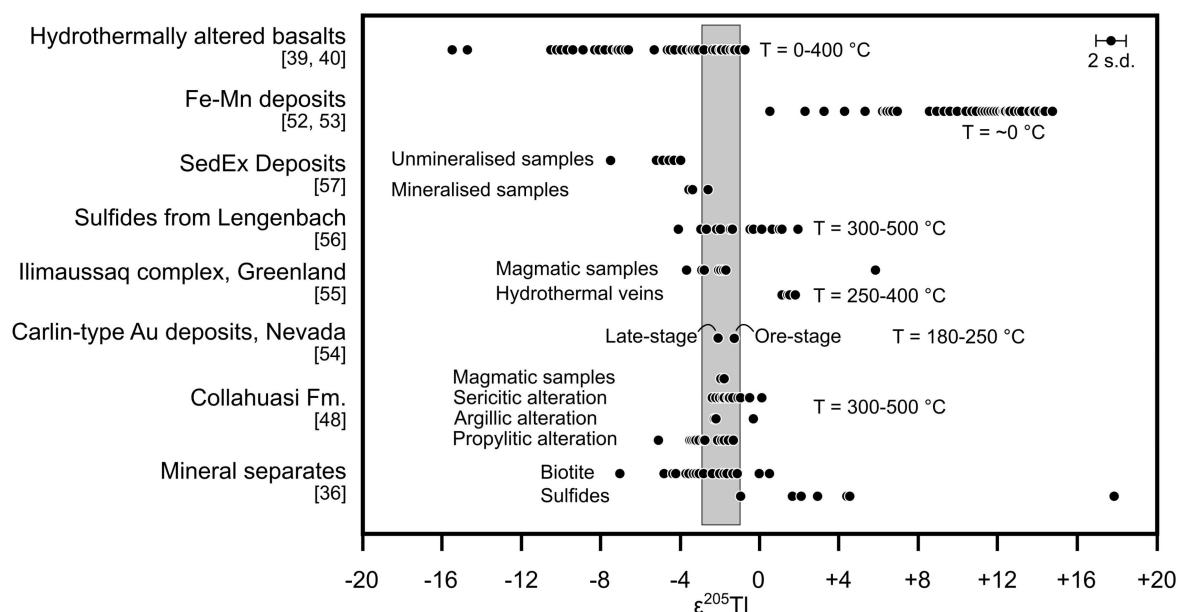


Figure 2. Summary of published Tl isotope ratios in hydrothermally altered basalts [39,40], Fe-Mn deposits [52,53], hydrothermal ore deposits [48,54–57], and mineral separates of biotite and sulfide from various geological environments [36]. The grey box represents the nominal mantle value of $\epsilon^{205}\text{Tl}$ (-2 ± 1 [31,41]); long-term external 2 s.d. reproducibility of several reference materials of ± 0.5 [31,42] shown as error bars for reference.

By contrast, Wickham [54] analysed ore- to late-stage sulfide samples from Carlin-type gold deposits in Nevada to determine the metal sources contributing to ore formation. Although no definitive conclusion was reached regarding the source(s) of Tl (and hence, Au), a negative shift in $\epsilon^{205}\text{Tl}$ values between ore-stage ($\epsilon^{205}\text{Tl} = -1.3$) and late-stage ($\epsilon^{205}\text{Tl} = -2.1$) sulfides (Figure 2) was interpreted to reflect the evolution of magmatic fluids, accompanied by mixing with either meteoric fluids or fluids derived from metamorphosed country rocks.

Hettmann et al. [55] analysed mineral separates from the Ilimaussaq complex, Greenland, to trace magmatic-hydrothermal processes using Tl isotope compositions. Most of their samples had $\epsilon^{205}\text{Tl}$ between -3 and $+2$, although one sample was enriched in the heavy ^{205}Tl isotope ($\epsilon^{205}\text{Tl} = +5.8$) and was inferred to be the result of alteration (Figure 2). Thallium concentrations varied from 0.03 – $350 \mu\text{g/g}$ and were higher in the hydrothermal regime compared to magmatic stages, implicating hydrothermal transport of Tl.

Hettmann et al. [56] examined mineral separates from the metamorphic Lengenbach Pb-As-Tl-Zn sulfide deposit, Switzerland, where relatively large Tl isotope fractionations ($\epsilon^{205}\text{Tl}$: -4.1 to $+1.9$) were observed. They suggested the large $\epsilon^{205}\text{Tl}$ range was related to crystallization of a variety of sulfide phases from a melt.

More recently, Peter et al. [57] conducted a bulk geochemical and Tl isotope study on samples from a sedimentary-exhalative (Sedex) Pb-Zn deposit in Canada, and found that “mineralized” samples displayed higher $\epsilon^{205}\text{Tl}$ values (-3.6 to -2.6) than “unmineralized” samples (-7.5 to -4.0 ; Figure 2). They also determined that the most likely Tl-hosting minerals were pyrite and sphalerite, due to correlations between Tl and Fe-S-Zn concentrations. Thallium abundances were also positively correlated with As-Hg-Sb concentrations, but not Pb.

Rader et al. [36] conducted the first systematic study to document Tl concentrations and $\epsilon^{205}\text{Tl}$ values of mineral separates from a variety of igneous, metamorphic, and metasomatic systems. In contrast to Peter et al. [57], they concluded that sulfides such as sphalerite and pyrite typically contain low or undetectable Tl. However, they also noted that, among co-existing minerals, sulfides and Fe-rich micas displayed the highest and lowest $\epsilon^{205}\text{Tl}$ values, respectively (Figure 2).

Based on the limited data that have been published to date, it can be concluded that samples from a variety of ore deposit types display Tl isotope fractionations that can be attributed to fluid evolution [54] or sulfide precipitation [36,55–57] (Figure 2). As a result, the current study aims to evaluate the potential of Tl isotopes for tracing fluid evolution, alteration, and sulfide precipitation in porphyry deposits by addressing the following questions: (1) Do Tl concentrations or $\epsilon^{205}\text{Tl}$ values correlate with elemental enrichments in porphyry deposits? (2) Can $\epsilon^{205}\text{Tl}$ be used to fingerprint hydrothermal fluids in porphyry systems? This latter question also permits examination of the possible genetic link between the Bingham Canyon porphyry system and the nearby sedimentary-hosted gold deposits of Barneys Canyon and Melco. The Bingham district was chosen for this study owing to previous reports of Tl-enrichment in late-stage gold mineralization (e.g., [11]) and its occurrence in the putative distal alteration halo [26]. Unlike the study of Baker et al. [48], the samples chosen for this study span a variety of lithologies from more distal areas of the Bingham district (up to 8.5 km away from the Bingham Canyon mine), which may help to elucidate Tl isotope behavior in the lower-temperature regimes of porphyry systems.

2. Materials and Methods

2.1. Samples

A comprehensive chemical database for 350 surface grab and drill core samples was compiled during an AMIRA International Ltd. (formerly Australian Mineral Industries Research Association) project (P1060), comprising major element compositions and the concentrations of 59 trace elements, including Tl. A subset of these data is presented in the Supplementary Material. Based on this larger sample suite, 19 samples comprising a variety of lithologies (Table 1) were selected for Tl isotope analysis.

Table 1. Thallium concentrations and isotope compositions in samples from the Bingham district, compared to standard reference materials; values of 2σ in *italics* originally returned values <0.6 , and were consequently assigned a more conservative value on the basis of multiple analyses of the Aldrich standard.

Sample	Lithology	Description	Tl _{WR} (ng/g)	$\epsilon^{205}\text{Tl}$	2σ	Tl (ng/g)	2σ	# Runs	# Sessions	# Dissolutions
Bingham Canyon										
BC11MB116	Sandstone	Weakly calcareous white sandstone on Middle Canyon Road	20	−4.2	<i>0.6</i>	88	11	4	2	1
BC11MB111	Silicified limestone	Silicified, grey Jordan limestone cut by thin calcite veinlets	450	−2.9	<i>0.6</i>	459	76	2	1	1
BC11MB101	Latite porphyry	Feldspar-phyrlic (\pm biotite) latite porphyry dyke with disseminated chlorite alteration	130	−8.8	<i>0.6</i>	1384	155	2	1	1
BC11MB102	Silicified limestone breccia	Brecciated, silicified limestone	1910	1.3	<i>0.6</i>	4932	47	2	1	1
BC11CW020	Quartzite	Massive, pale grey, fine-grained quartzite	210	0.9	1.1	274	20	3	2	1
BC12LZ527	Latite porphyry	Latite porphyry with K-feldspar altered plagioclase, strong propylitic alteration and quartz-pyrite veins	700	−2.9	<i>0.6</i>	1687	78	3	2	1
BC11DC007c	Lamprophyre	Lamprophyre containing minor bornite and chalcocopyrite and late quartz-calcite veins	820	−3.6	<i>0.6</i>	1525	124	5	1	1
BC11DC005a	Monzonite	Propylitically-altered monzonite, with early barren quartz veins cut by quartz-molybdenite-Cu-Fe-sulfide veins (5–20 mm wide)	860	−1.3	<i>0.6</i>	1420	85	4	1	1
BC12JT601	Recrystallised calcareous sandstone	Weakly-bedded, recrystallised, and fractured calcareous sandstone, containing calcite-pyrite veins	120	−3.3	<i>0.6</i>	207	30	3	2	1
BC11MB155	Silicified limestone	Silicified limestone from above Northern Haul Road, cut by numerous thin (up to 1 cm) coarse crystalline calcite veins	30	0.2	0.8	256	23	5	1	1
BC11MB152b	Quartzite	Quartzite from layer below limestone; contains spots of red-brown mineral, possibly Fe-carbonate-after-pyrite	90	−3.4	<i>0.6</i>	341	5	3	2	1
BC11MB151	Quartzite	Massive quartzite	50	−1.5	<i>0.6</i>	138	14	2	1	1
BC11MB146	Quartzite breccia	Quartzite breccia, with angular to sub-rounded quartzite clasts in calcite-dominated crystalline cement	4790	7.2	1.8	7213	1108	2	1	1
BC11DC164	Quartzite breccia	0.5 m-wide breccia zone in quartzite surrounding shear band; clayey matrix obscures clast-matrix/cement relationship	120	−2.3	<i>0.7</i>	358	12	3	2	1
Barneys Canyon/Melco										
BC11CW089b	Veined limestone	Dark grey limestone with stockwork of calcite veins (between 1–10 mm in width)	31590	−6.5	<i>0.6</i>	5072	634	2	1	1
BC11MB184	Quartzite breccia	Silicified, solution-collapse breccia in quartzite, located immediately NE of Melco pit	790	6.0	<i>0.6</i>	698	33	4	2	1

Table 1. Cont.

Sample	Lithology	Description	Tl _{WR} (ng/g)	$\epsilon^{205}\text{Tl}$	2 σ	Tl (ng/g)	2 σ	# Runs	# Sessions	# Dissolutions
Barneys Canyon/Melco										
BC11MB185	Quartzite breccia	Brecciated quartzite containing discontinuous calcite veinlets;	1270	−16.4	0.7	1545	137	7	2	2
BC11CW079	Quartzite	Pale beige, hard, finely crystalline quartzite containing stockwork of quartz veinlets (0.5–2 mm wide) from Barney's Canyon mine, sampled away from most intense clay alteration and fracturing	1780	−3.1	0.6	824	19	2	1	1
BC11CW080b	Dolomitic nodule	Possibly bituminous dolomite nodules with large (up to 10 cm) open cavities with inwards-growing calcite crystals (up to 4 mm long)	6080	0.0	0.6	4650	499	2	1	1
Standards										
AGV-2 (this study)				−2.8	0.5	271	92	2	2	2
AGV-2 [43]				−3.0	0.6	267	35	15	n/a	8
Aldrich (this study)				−0.8	0.6	n/a	n/a	36	2	n/a
Aldrich [31]				−0.8	0.3	n/a	n/a	133	n/a	n/a

2.2. Whole Rock Geochemistry

Bulk-rock geochemical analyses for major and trace elements were carried out by ACME Analytical Laboratories Ltd. (now Bureau Veritas Commodities Canada Ltd.) in Vancouver, Canada. Samples were crushed using a jaw crusher, before being powdered (95% passing <100 µm) using a ceramic rod pulverizer. Approximately 0.2 g of each sample was mixed with 1.5 g of lithium metaborate/lithium tetraborate flux in a graphite crucible, before being fused at 980 °C for 30 min. The fused sample was then dissolved in 5% HNO₃. Major element compositions were obtained using a Jarrel-Ash AtomComp Model 975 (Waltham, MA, USA)/Spectro Ciros Vision (Kleve, Germany) inductively-coupled-plasma optical emission spectrometer (ICP-OES).

Another cut of the powdered sample was dissolved in a mixture of H₂O-HF-HClO₄-HNO₃. The solution was evaporated to dryness, and dilute HCl was subsequently added for analysis, which was conducted using a Perkin-Elmer Elan 6000 or 9000 (Boston, MA, USA) inductively-coupled-plasma mass spectrometer (ICP-MS). The detection limits are 0.04 wt.% for major elements and 0.5 µg/g for most trace elements (except the rare earth elements: 0.05 µg/g).

2.3. Chemical Separation of Tl

Samples for Tl isotope analysis were sourced from rocks collected close (within ~10 cm) to where whole-rock geochemical samples were obtained. These samples were dissolved using conventional acid digestion methods [3:1 HF:HNO₃], and Tl was separated by a two-stage ion chromatography procedure as described by Rehkamper and Halliday [58] and refined by Nielsen et al. [59] (Figure 3). Thallium isotope measurements were performed using a Nu Instruments (Wrexham, UK) multiple-collector inductively-coupled-plasma mass spectrometer (MC-ICP-MS) in the MAGIC laboratories at Imperial College London.

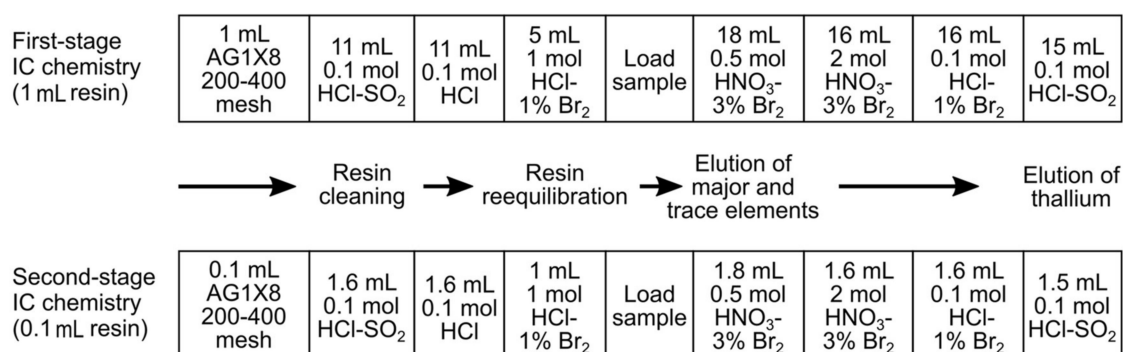


Figure 3. A flowchart showing the Tl separation column chromatography process, modified after [59].

2.4. MC-ICP-MS Protocols

Thallium concentrations in rock powders were determined during MC-ICP-MS (utilizing the known concentration of Pb added to solutions), thus allowing comparison with ICP-MS determinations from adjacent whole-rock samples. For Tl isotope measurements, a solution of 0.1 mol HNO₃-0.1% H₂SO₄ was prepared for the dilution of all samples and standards to minimize possible matrix effects (see [59]). Because Tl has only two stable isotopes, samples were doped with a known amount of NIST SRM981 Pb solution to correct for instrumental mass bias [58]. Sample solutions were run at Pb/Tl ratios of between 2.4–3.9 and contained 2–6 ng/g Tl. Samples were measured by sample-standard bracketing with NIST SRM997 Tl, which is defined as $\epsilon^{205}\text{Tl} = 0$. A secondary Tl solution standard from Sigma Aldrich was interspersed with unknown samples. The Aldrich solution standard has been run by multiple laboratories over the last decade ($\epsilon^{205}\text{Tl} = -0.8 \pm 0.3$, 2 s.d.; [31,42]) and provided additional quality control. Machine performance was considered acceptable when the variation between bracketing NIST SRM997 Tl solutions was $<4 \times 10^{-5}$ and the Aldrich solution returned $\epsilon^{205}\text{Tl}$ within its documented long-term reproducibility. Concentrations of Pb and Tl in the samples

were matched to within 15% of their concentrations in the bracketing standards in order to minimize possible matrix effects.

3. Results

3.1. Data Quality Assessment: Reference Materials, Solution Standards and Total Procedural Blanks

Data accuracy and precision were assessed using USGS andesitic reference material AGV-2, which has been characterized for its Tl concentration and isotope composition [33,43,60] and was dissolved and measured as an unknown during each MC-ICP-MS session. The secondary standard Aldrich solution was also measured as an unknown at the beginning and end of each analytical session to assess further the accuracy and precision of the isotope measurements. Results for the standards are given in Table 1 and are within error of accepted values. Total procedural blanks yielded 10–15 mV Pb (~50 pg/g) and Tl at electronic background levels (3 mV, ~6 pg/g).

3.2. Thallium Concentrations Measured by MC-ICP-MS vs. ICP-MS

Sample Tl concentrations analysed by the two different methods scatter around a 1:1 line (Figure 4). Small differences in Tl content are likely due to MC-ICP-MS concentration estimates being made on a different powder from an adjacent sample to the trace element determinations from the AMIRA project. This implies some heterogeneity of Tl concentrations on the hand sample scale. Where available, concentration data from the MC-ICP-MS measurements are used in any figures henceforth, as they were obtained from the same powder and dissolution as the isotope data.

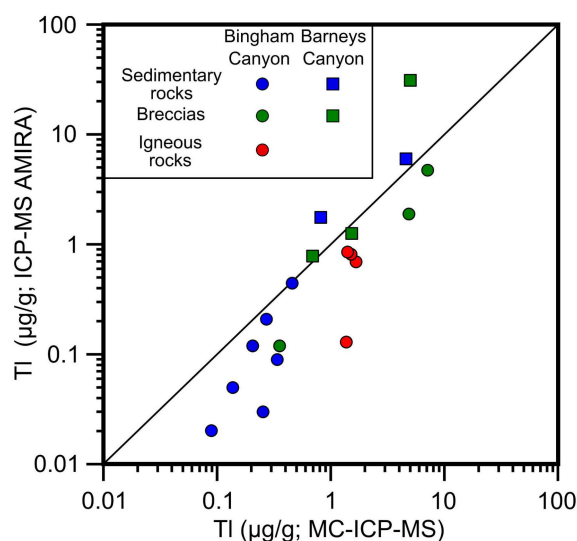


Figure 4. A plot of Tl concentrations ($\mu\text{g/g}$) measured by ICP-MS (during the AMIRA project (P1060)) compared to MC-ICP-MS (this study); 1:1 line provided for reference.

3.3. Thallium Concentrations as a Function of Sample Type and Location

Overall, Tl concentrations do not show strong correlations with other elements (Figure 5). The strongest correlations are with alkali metals (e.g., K_2O -Tl Spearman Rank correlation coefficient = 0.49). A box-and-whisker plot of Tl concentrations subdivided according to rock type (Figure 6) shows that there is slight enrichment in Tl in more evolved igneous rocks, consistent with the incompatible behavior of Tl during magmatic fractionation. The igneous rocks that form part of the Bingham intrusive complex are also generally enriched in Tl relative to the surrounding sedimentary host rocks (Figure 6). It is noteworthy, however, that most samples from the district are at or below the average abundance of Tl in the continental crust (0.5–1.6 $\mu\text{g/g}$; [61]). Of the sedimentary host rock lithologies, dolomite, siltstone, and sandstone display the highest Tl concentrations (median concentrations of

0.21, 0.12, and 0.11 $\mu\text{g/g}$, respectively). However, these samples are located in the north, in the area associated with the Melco and Barneys Canyon hydrothermal systems (i.e., the Permian sedimentary rocks in Figure 1; [12,23]). Of greatest significance is the fact that hydrothermal breccias are generally enriched in Tl relative to their coherent sedimentary counterparts (Figure 6).

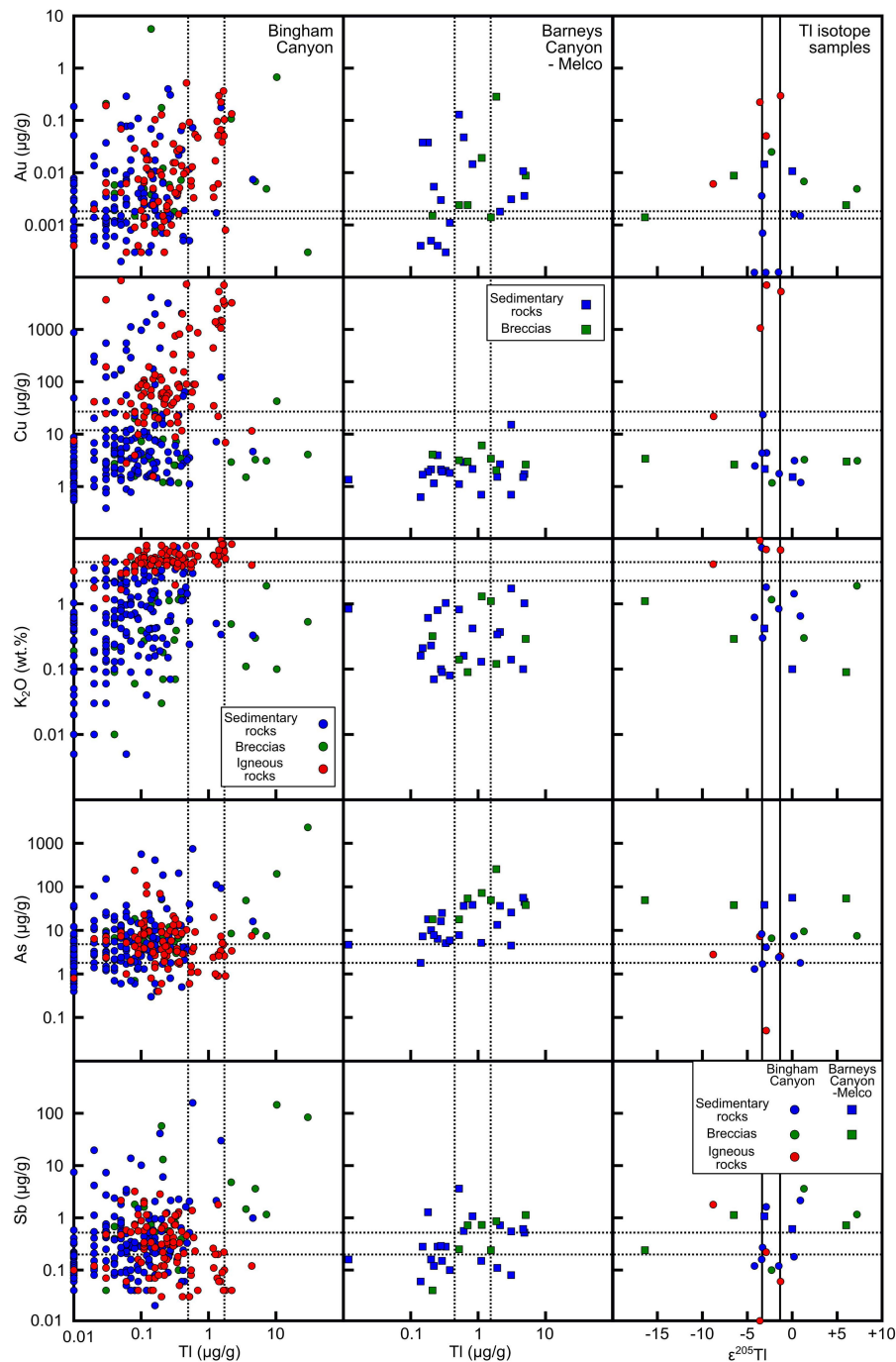


Figure 5. Plots of Au ($\mu\text{g/g}$), Cu ($\mu\text{g/g}$), K_2O (wt.%), As ($\mu\text{g/g}$), and Sb ($\mu\text{g/g}$) against Tl ($\mu\text{g/g}$) and $\epsilon^{205}\text{Tl}$ values measured in this study for the Bingham Canyon area (left column), the Barneys Canyon-Melco area (centre) and for samples analysed for Tl isotopes (right column); symbols as in Figure 4; dotted lines indicate range of continental crust abundance estimates [61]; solid lines in $\epsilon^{205}\text{Tl}$ plots indicate mantle range [31,41]; geochemical data reported in the Supplementary Material.

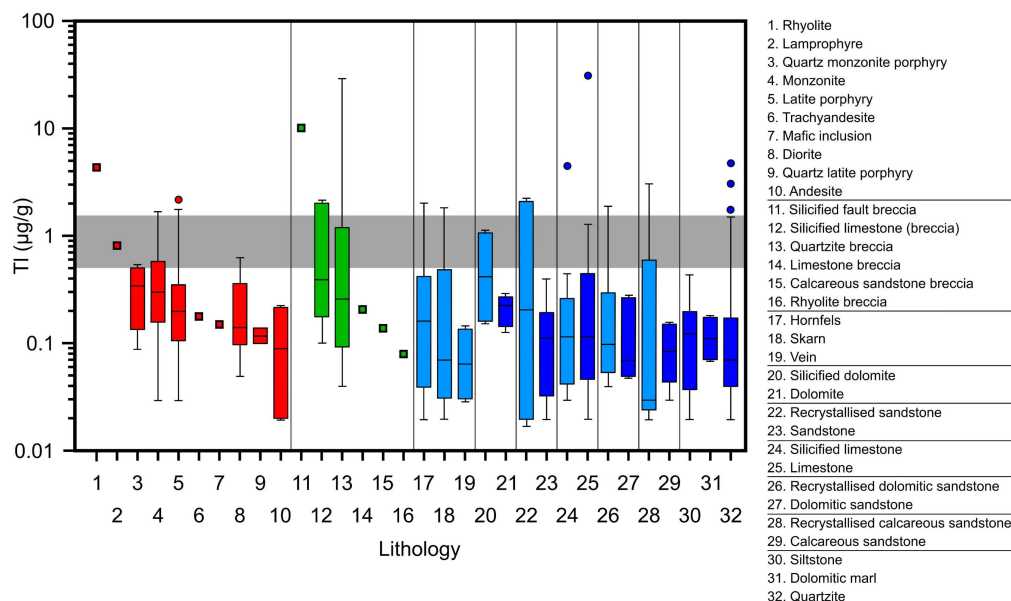


Figure 6. A box and whisker plot showing Tl abundance by lithology in all samples ($n = 350$) from the Bingham district, with samples grouped into broad lithological categories. “Boxes” denote the first and third quartile values, while the intermediate lines indicate median Tl contents; whiskers extend to the highest and lowest values, excluding outliers (circles), which are >1.5 times the inter-quartile range higher and lower than the third quartile and first quartile measurements, respectively; the solid squares indicate one measurement for a given lithology; colors as in Figures 4 and 5; pale blue color indicates recrystallized/silicified sedimentary lithologies. Note log-scale on y -axis; shaded box indicates range of estimates for Tl content of bulk continental crust [61].

3.4. Thallium Isotope Compositions

Table 1 shows Tl concentration and isotope ratio data for the subset of samples analysed for Tl isotopes from the Bingham district. The range in Tl isotope compositions reported here is compared with results from previous studies in Figure 7.

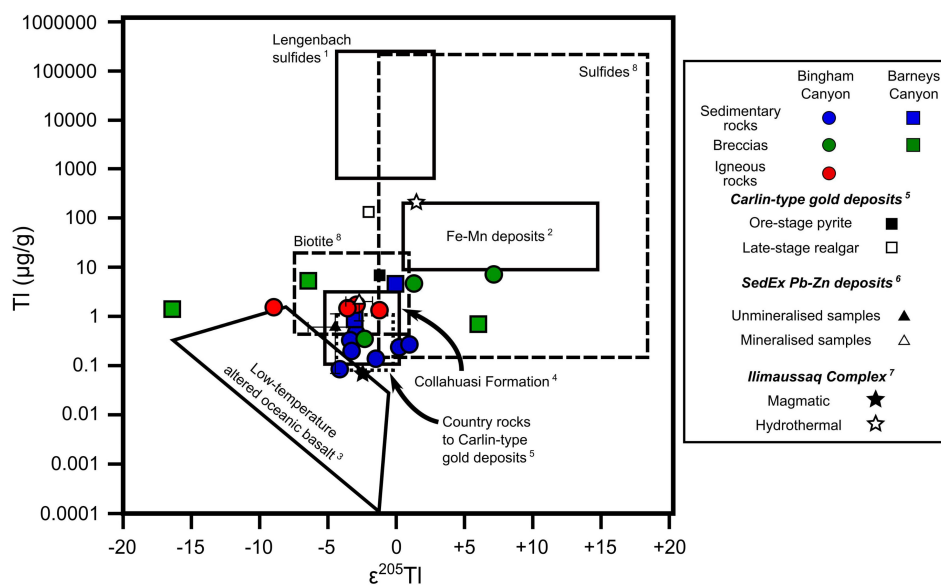


Figure 7. A plot of Tl concentration ($\mu\text{g/g}$) vs $\epsilon^{205}\text{Tl}$ in samples from the Bingham Canyon district (this study) compared to literature data: ¹ [56]; ² [52,53]; ³ [39,40]; ⁴ [48]; ⁵ [54]; ⁶ [57]; ⁷ [55]; ⁸ [36].

3.4.1. Bingham Canyon

Thallium isotope compositions of samples from Bingham Canyon show significant variations ($\epsilon^{205}\text{Tl}$ from -8.8 to $+7.2$). However, three igneous samples closest to the Bingham Canyon mine display a narrow range of $\epsilon^{205}\text{Tl}$ (-3.6 to -1.3), resembling the mantle range ($\epsilon^{205}\text{Tl} = -2.0 \pm 1.0$). Unbrecciated sedimentary samples ($n = 7$) also display a limited range in $\epsilon^{205}\text{Tl}$ (between -4.2 and $+0.9$). These compositions contrast with that of a latite dyke sample from the southwest of the Bingham district, which has anomalously low $\epsilon^{205}\text{Tl}$ ($= -8.8$), and brecciated samples, which have much more variable $\epsilon^{205}\text{Tl}$ (-2.3 to $+7.2$).

3.4.2. Barneys Canyon and Melco

Five samples from the area surrounding the sediment-hosted gold systems were analysed. The $\epsilon^{205}\text{Tl}$ range in these samples (-16.4 to $+6.0$) is significantly greater than at Bingham Canyon. All of this variability occurs in brecciated or veined samples; by contrast, unbrecciated sedimentary samples have similar $\epsilon^{205}\text{Tl}$ values (-3.1 to $+0.0$) to unbrecciated samples from Bingham Canyon (Figures 5 and 7).

4. Discussion

The relationship between spatial position, pathfinder metal concentrations such as Cu (that are typically zoned in whole rock data from porphyry systems), $\epsilon^{205}\text{Tl}$, and Tl concentrations is key to understanding Tl transport in porphyry fluids and evaluating the potential of Tl as a vectoring tool. Furthermore, there is scope in the dataset to potentially distinguish between the porphyry hydrothermal system and distal, low temperature hydrothermal systems that may or may not be associated with it. Comparisons are first drawn between Tl concentrations and isotope fractionations at Bingham Canyon, USA, and the only previous study of Tl in a porphyry Cu system in Chile [48]. The overall variabilities of both Tl content and isotope ratios in the Bingham district are then discussed, before the potential for using Tl isotopes as a vectoring tool is assessed. Factors controlling Tl isotope fractionations are also examined, including the possible composition and aqueous species of the Barneys Canyon hydrothermal fluids.

4.1. Comparison between Bingham Canyon, USA, and Collahuasi Formation, Chile

There has only been one previous study of Tl isotope variations in a porphyry Cu system, which examined the Collahuasi Formation in Chile, i.e., the host rocks to the Collahuasi cluster of deposits [48]. In this area, where the principal host rocks are all igneous, Tl showed strong lithophile affinities. Similarly, in the Bingham district, Tl abundances are also most strongly correlated with alkali metals such as K (Figure 5). This again suggests that Tl behaves predominantly as a lithophile element, likely substituting into minerals such as biotite and K-feldspar, consistent with the data presented by Baker et al. [48]. In contrast, there is no correlation in any lithology at Bingham Canyon between Tl abundances and chalcophile elements or ore metals (Figure 5), suggesting that Tl behavior in this location is not simply linked to the distribution of Cu, and will not provide a direct means of tracing Cu ore precipitation, supporting the conclusions of Baker et al. [48]. The general Tl-enrichment of the more evolved igneous rocks at Bingham Canyon (Figure 6) suggests that the dominant control on elevated Tl concentrations in this location is the incompatibility of Tl during magmatic processes.

The range of $\epsilon^{205}\text{Tl}$ values from the Collahuasi Formation (-5.1 to $+0.1$; [48]) is very similar to the range found in unbrecciated sedimentary and igneous samples from Bingham Canyon (-4.2 to $+0.9$; Figure 7). Furthermore, igneous samples at Bingham Canyon (excluding the anomalous latite sample) have $\epsilon^{205}\text{Tl}$ values (-2.6 ± 2.3 , 2 s.d.) and Tl abundances (1544 ± 135 ng/g) that fall within the range of values from the Collahuasi Formation [48] (Figure 7). It can therefore be concluded that there is limited fractionation of Tl isotopes during high temperature igneous and/or hydrothermal processes.

4.2. Variability in Tl Abundance and $\epsilon^{205}\text{Tl}$ throughout the Bingham District

The overall range in $\epsilon^{205}\text{Tl}$ observed in samples from the Bingham district (~ 24 ϵ units) is almost double what has been previously observed in hydrothermally altered basalts (~ 15 ϵ units) and in Fe-Mn deposits (~ 14 ϵ units; Figure 7). Moreover, samples from the Bingham district display both positive and negative excursions in $\epsilon^{205}\text{Tl}$ from the mantle value (-2.0 ± 1.0 ; [41]). Most of the variability in $\epsilon^{205}\text{Tl}$ is found in samples further away from the Bingham Canyon porphyry intrusions (Figure 8), and most of the extreme $\epsilon^{205}\text{Tl}$ values were observed in breccia samples from both the Bingham Canyon (-2.3 to $+7.2$) and Barney's Canyon areas (-16.4 to $+6.0$; Figure 7). Breccia samples also display a wide range of Tl concentrations (360–7200 ng/g; Figure 6; Table 1). The extreme variations in both $\epsilon^{205}\text{Tl}$ and Tl concentration in breccia samples suggest a strong control on Tl behavior by the nature (P–T–x properties) of the fluids involved in breccia formation.

There are three breccias from the Bingham Canyon area that display a wide range in $\epsilon^{205}\text{Tl}$ values (from -2.3 to $+7.2$). The sample with a mantle-like $\epsilon^{205}\text{Tl}$ value (BC11DC164) comes from a brecciated zone around a clayey shear band (Table 1), and is therefore interpreted to reflect fragmentation of the pre-existing country rock (quartzite) in a fault zone, rather than having any hydrothermal influence. The other two breccia samples from the Bingham Canyon area, which are distinct in having both high Tl contents (4932–7213 ng/g) and unusual, high $\epsilon^{205}\text{Tl}$ ($+1.3$ to $+7.2$; Figure 7), are both cemented breccias with matrices of quartz and/or calcite.

One sample from a latite dyke ~ 2 km to the southwest of the Bingham Canyon mine (BC11MB101) has anomalously low $\epsilon^{205}\text{Tl}$ (-8.8), which is not consistent with the other igneous rocks analysed in this study or by Baker et al. [48]. This sample also has a different major and trace element composition relative to the other analysed magmatic samples, with higher Sb, and lower K_2O , Cu, and Au contents (Figure 5). It is notable that this sample occurs beyond the zone of proximal porphyry alteration and mineralization at Bingham Canyon [62], and the presence of chlorite (illite) indicates that it has undergone lower temperature propylitic alteration. Without further detailed investigation, it is not possible to infer the exact cause, but we suggest that low temperature alteration (200 – 300 $^\circ\text{C}$) has resulted in Tl isotope fractionation in this sample, with preferential mobilization of ^{205}Tl out of altered K-feldspar and/or biotite, accompanied by K removal. This isotopic shift may have been exacerbated by pre-existing ^{203}Tl -enrichment in biotite (Figures 2 and 7; [36,42]).

Although Tl concentrations and isotope compositions are not directly related to other common proximal indicators of porphyry deposits (e.g., Cu or Au concentrations, K-enrichment due to potassic alteration; Figure 5), it may instead be possible to use Tl isotope ratios to enhance the characterization of geochemical halos in the more distal areas surrounding porphyry deposits. In the Bingham district, samples displaying large $\epsilon^{205}\text{Tl}$ excursions coincide with elevated abundances of Tl (Figure 7) and other chalcophile elements (e.g., As, Sb; Figure 5) that are typically enriched in low temperature hydrothermal systems (e.g., [8,63]). The enrichment in Tl and greater variability in $\epsilon^{205}\text{Tl}$ values also correlate with hydrothermally brecciated zones involving calcite and quartz cements, silicification and/or veining, with crustiform textures generally suggestive of low temperature, epithermal conditions. These breccias may be linked to late-stage and/or more distal, low-temperature hydrothermal fluid activity, potentially responsible for the gold mineralization in the Barney's Canyon-Melco area to the north of Bingham Canyon (Figures 7 and 8; Table 1).

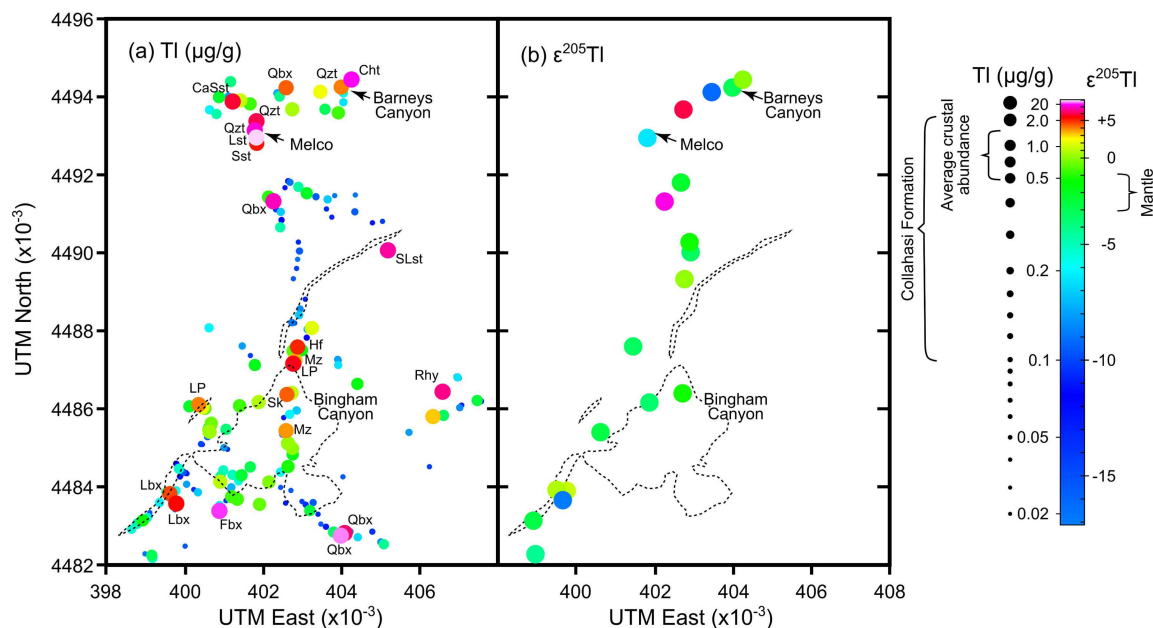


Figure 8. Map of sample locations in the Bingham district, showing (a) Tl concentration (μg/g) and (b) $\epsilon^{205}\text{Tl}$ value in all analysed samples, using color (a,b) and symbol size (a only); ranges in concentration for the bulk continental crust (values from [61]) and in rocks from the Collahuasi Formation (values from [48]) are also marked on the key for reference, as is the range of $\epsilon^{205}\text{Tl}$ for the mantle [31,41]; dashed lines delineate the extents of the main intrusive bodies of the Bingham complex; locations of Melco and Barneys Canyon mines also shown; samples with high Tl concentrations are shown with abbreviated lithologies as follows: CaSst = calcareous sandstone; Cht = chert; Fbx = fault breccia; Hf = hornfels; Lbx = limestone breccia; LP = latite porphyry; Lst = limestone; Mz = monzonite; Qbx = quartzite breccia; Qzt = quartzite; Rhy = rhyolite; Sk = skarn; SLst = silicified limestone; Sst = sandstone.

4.3. Thallium Behavior in Sediment-Hosted Gold Systems

Samples from the northern part of the Bingham district display a large range in $\epsilon^{205}\text{Tl}$ (from -16.4 to $+6.0$; Figure 7), in addition to a general enrichment in Tl (Figure 8). The variations in $\epsilon^{205}\text{Tl}$ in the Barneys Canyon-Melco area are positively correlated with Sb abundances, and negatively correlated with K abundances (Figure 5). Excursions in $\epsilon^{205}\text{Tl}$ may therefore be related to variable Tl-partitioning behavior between K-bearing silicate phases and sulfides that may be more closely related to low temperature gold mineralization than to porphyry ore-forming processes.

Thallium isotope ratios can also be affected by kinetic processes during boiling (e.g., [31]); however, Presnell and Parry [12] found no evidence for boiling in fluid inclusions at Barneys Canyon. Other processes that result in kinetic fractionation are not necessarily constrained in the context of Tl isotopes. Baker et al. [60] examined the effects of volcanic degassing, evaporation, and condensation on Tl isotopes by analysis of volcanic gas condensates and particulates. They found no systematic direction of kinetic isotope fractionation, and instead proposed a counterbalance between the processes of evaporation, which creates an isotopically light gas phase, and condensation during gas cooling, which creates an isotopically heavy residual vapor phase. The lack of systematic behavior (i.e., excursions in $\epsilon^{205}\text{Tl}$ to both positive and negative values; Figures 7 and 8) in the Barneys Canyon-Melco area could, in principle, be explained by kinetic fractionation processes of this kind involving volcanic gas interactions with meteoric water.

The variability in both Tl concentration and isotope composition observed in this study may also have been caused by hydrothermal fluid evolution that led to changes in parameters such as temperature, pH, or $f\text{O}_2$. Thallium isotope fractionations have been closely linked to temperature (e.g., [39]) and redox conditions (e.g., [57]), so any proposed model must assess these factors. Fluid inclusion homogenization temperatures are lower at Barneys Canyon than at Bingham Canyon,

with measurements falling between 130–390 °C and an inferred maximum temperature at Barneys Canyon of 280 °C [12]. By contrast, Cunningham et al. [23] suggested that the Barneys Canyon area did not experience temperatures greater than ~120 °C.

Xiong [64] attempted to quantify the relative concentrations of anionic species transporting Tl in oxidizing and reducing solutions at temperatures ≤ 300 °C, making this relevant to the conditions extant during low-temperature gold mineralization in the Bingham district. The low-salinity (i.e., low concentration of Cl^-) and weakly acidic nature of the solutions that form such peripheral gold deposits [6,65] implies a pH range between 5 and 7. Under these conditions, and considering all possible fluid temperatures between 100–300 °C, HS^- theoretically dominates Tl transport in hydrothermal fluids (Figure 9; [64]); this is analogous to Au behavior (e.g., [65]). Some fluid inclusions in samples from Barneys Canyon were found to have high H_2S concentrations [65], supporting the notion that Tl (together with Au) could have been transported to Barneys Canyon–Melco by complexation with HS^- . Increased abundances of other “low temperature” chalcophile elements (e.g., As) in the Barneys Canyon–Melco area (Figure 5) further support Tl-transport to this location in a sulfur-rich fluid phase.

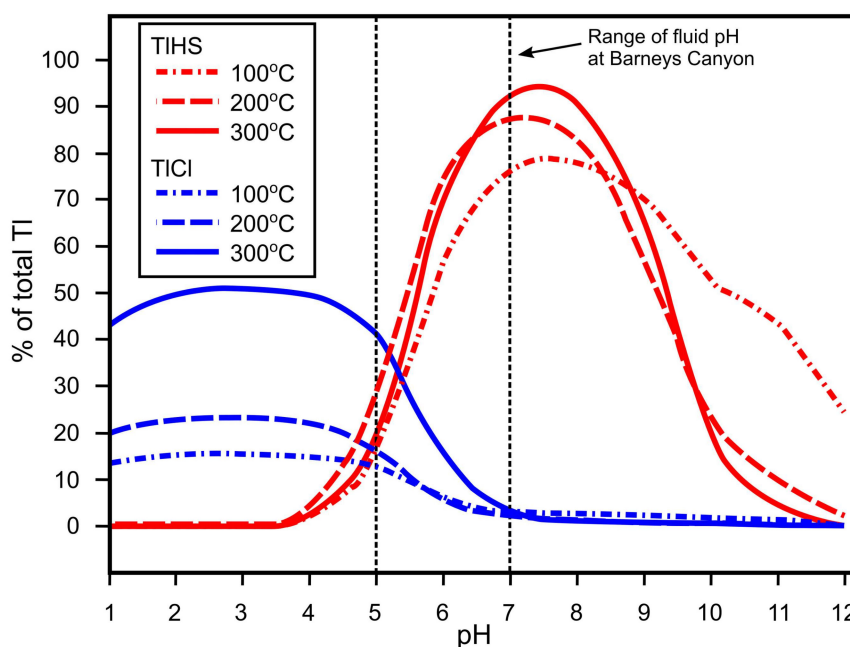


Figure 9. Modelled % of total Tl transported by Cl^- and HS^- anions in hydrothermal fluids plotted against fluid pH in reducing conditions at temperatures between 100–300 °C; modified after [63].

A variety of sulfide minerals, which may occur at the centre of disseminated gold deposits like Barneys Canyon [12,66,67], have been found to incorporate Tl. Arehart et al. [67] noted that As-sulfides—including realgar (AsS), orpiment (As_2S_3), and galkhaite $[(\text{Cs},\text{Tl})(\text{Hg},\text{Cu},\text{Zn})_6(\text{As},\text{Sb})_4\text{S}_{12}]$ —typically occur in Carlin-type deposits, albeit late in the Au-mineralization stage. Whereas galkhaite contains Tl as a major element, orpiment can contain high Tl contents (850 $\mu\text{g/g}$), and realgar minor quantities (0.2 $\mu\text{g/g}$; [36]; or 127 $\mu\text{g/g}$; [54]). Variable $\epsilon^{205}\text{Tl}$ at Barneys Canyon may therefore be related to the localized precipitation and segregation of different Tl-bearing sulfides, or more likely during Tl-accumulation as a trace element in other, more abundant sulfide phases [36,54]. Such a mechanism would be reflected by equilibrium isotope fractionation driven by the contrasting co-ordination (i.e., bonding environment) of Tl with anions (such as Cl^- and S^{2-}) in magmas, aqueous fluids, and the precipitating minerals [56]. Control on isotope fractionation by the precipitation of Tl-rich minerals is supported by large $\epsilon^{205}\text{Tl}$ variations (19 ϵ units) in sulfides from assorted hydrothermal ore deposits [36], and a smaller yet still significant range of ~6 ϵ units in sulfides from the Lengenbach deposit [56] (Figures 2 and 7).

Although Tl behaves differently at Bingham Canyon compared to the Barneys Canyon–Melco area, the data presented herein do not provide conclusive evidence regarding a genetic relationship between the two. The causes of the variability in Tl behavior remain uncertain: kinetic processes associated with vapor separation cannot be definitively dismissed, but the effect of contrasting bonding environments of Tl-rich sulfide minerals with the low temperature hydrothermal fluids from which they precipitate likely plays a dominant role.

5. Outlook

This reconnaissance study investigated the range of Tl isotope ratios in a well-characterized porphyry district (Bingham Canyon and neighbouring low temperature gold deposits). Although no relationship is evident between Tl isotopes and porphyry deposit pathfinder elements, brecciated and veined samples display significant excursions from the mantle $\epsilon^{205}\text{Tl}$ value to both positive and negative values, most likely caused by the volatility of Tl, kinetic isotope effects, or more broadly due to interactions with low-temperature hydrothermal fluids.

Individual mineral separates have been shown to have analytically significant variations in $\epsilon^{205}\text{Tl}$ values [36]; such a study could be conducted on samples from Bingham Canyon to determine (1) which phases host the highest Tl concentrations; and (2) whether anomalous $\epsilon^{205}\text{Tl}$ values or concentrations of Tl are associated with specific Tl-bearing minerals, or are linked to Tl substitution within sulfides. Importantly, it is now analytically feasible to analyze multiple isotope systems—which may provide information on fluid speciation (e.g., O–Cl–S, together with Tl)—on the same materials as bulk-rock analysis and mineralogical characterization.

6. Conclusions

Samples from the Bingham Canyon district in Utah, USA, document the largest range in $\epsilon^{205}\text{Tl}$ (−16.4 to +7.2) observed in hydrothermal ore deposits to date. This range in $\epsilon^{205}\text{Tl}$ (~24 ϵ units) also surpasses the variability that has previously been observed in both hydrothermally altered basalts (~15 ϵ units) and Fe–Mn crusts (~14 ϵ units). The locally high (up to ~30,000 ng/g; see Supplementary Material) and variable Tl concentrations in samples analysed in this study are also uncommon and warrant further investigation of the mineral phases that host Tl.

Thallium appears to behave in a lithophile manner in igneous samples at Bingham Canyon, which is suggested to be a result of its incompatibility during magmatic processes and the similarities between Tl^+ and alkali metal ions. Thallium isotope fractionations at Bingham Canyon cannot be directly related to other geochemical enrichments that would ordinarily be associated with ore formation, or potassic alteration. Instead, the data presented here are consistent with limited fractionation of Tl isotopes during high temperature igneous and/or hydrothermal processes.

In contrast, samples from the Barneys Canyon–Melco area, and from breccia samples throughout the district, show positive correlations between Tl and chalcophile elements such as As and Sb, which may relate to low temperature hydrothermal activity linked to sediment-hosted gold mineralization. Theoretical considerations, coupled with fluid inclusion analyses, suggest Tl and Au could have been co-transported to the Barneys Canyon–Melco area as bisulfide (HS^-) complexes, consistent with increased levels of chalcophile elements in this location. The extraordinary range in $\epsilon^{205}\text{Tl}$ from −16 to +7 in breccia samples from the Bingham district further supports a strong control on $\epsilon^{205}\text{Tl}$ variability by low temperature hydrothermal fluid activity. Kinetic processes, which may relate to vapor separation during hydrothermal fluid evolution, cannot be definitively dismissed as the cause of Tl isotope variability; however, Tl-rich sulfide precipitation also appears to be a strong candidate for fractionating Tl isotopes.

Further analysis to determine the mineral phase(s) hosting Tl and extreme Tl isotope signatures offers a fruitful avenue of future research. Combining such findings with analyses of other stable isotope systems on the same material is a potentially powerful approach to elucidate fluid complexation routes in the final cooling of hydrothermal fluids that generate ore deposits.

Supplementary Materials: Selected major and trace element contents in bulk-rock samples from AMIRA project P1060.

Author Contributions: J.P. and J.J.W. conceived the project; A.F. and J.P. performed the experiments; A.F. analysed the data; J.J.W., D.R.C., M.J.B., C.C.W. contributed the samples; and A.F. wrote the paper (assisted by all other authors).

Funding: Samples were collected during the AMIRA P1060 research project, funded by a consortium of industry sponsors.

Acknowledgments: This study was undertaken as part of AF's Master's research project at Imperial College London. The authors acknowledge the assistance of Barry Coles and Alex Brett, who helped throughout analytical sessions. We also thank Janet Hergt (University of Melbourne) for her generosity, Kim Schroeder (Rio Tinto) for his help and advice during this project, and Jennifer Thompson and Lejun Zhang (both TMVC/CODES) for collecting additional samples used in this study. An early version of this manuscript benefited from informal reviews by R. Sievwright and E. Spencer. We are also grateful for extremely efficient editorial handling and constructive comments from four anonymous reviewers. The entire MAGIC research group at Imperial College London, and particularly Katharina Kreissig, are thanked for their overwhelming support.

Conflicts of Interest: The authors declare no conflict of interest. The funding sponsors had no role in the design of the study; in the collection, analyses, or interpretation of data; in the writing of the manuscript, and in the decision to publish the results.

References

1. Sillitoe, R.H. Porphyry copper systems. *Econ. Geol.* **2010**, *105*, 3–41. [\[CrossRef\]](#)
2. Tosdal, R.M.; Dilles, J.H.; Cooke, D.R. From source to sinks in auriferous magmatic-hydrothermal porphyry and epithermal deposits. *Elements* **2009**, *5*, 289–295. [\[CrossRef\]](#)
3. Richards, J.P. Tectono-magmatic precursors for porphyry Cu-(Mo-Au) deposit formation. *Econ. Geol.* **2003**, *98*, 1515–1533. [\[CrossRef\]](#)
4. Wilkinson, J.J. Triggers for the formation of porphyry ore deposits in magmatic arcs. *Nat. Commun.* **2013**, *6*, 917–925. [\[CrossRef\]](#)
5. Sillitoe, R.H.; Hedenquist, J.W. Linkages between volcanotectonic settings, ore-fluid compositions, and epithermal precious metal deposits. *Spec. Publ. Soc. Econ. Geol.* **2003**, *10*, 315–343.
6. Heinrich, C.A.; Driesner, T.; Stefansson, A.; Seward, T.M. Magmatic vapor contraction and the transport of gold from the porphyry environment to epithermal ore deposits. *Geology* **2004**, *32*, 761–764. [\[CrossRef\]](#)
7. Hemley, J.J.; Hunt, J.P. Hydrothermal ore-forming processes in the light of studies in rock-buffered systems: II. Some general geologic applications. *Econ. Geol.* **1992**, *87*, 23–43. [\[CrossRef\]](#)
8. Sillitoe, R.H.; Bonham, H.F., Jr. Sediment-hosted gold deposits: Distal products of magmatic-hydrothermal systems. *Geology* **1990**, *18*, 157–161. [\[CrossRef\]](#)
9. Cooke, D.R.; Hollings, P.; Walshe, J.L. Giant porphyry deposits: Characteristics, distribution, and tectonic controls. *Econ. Geol.* **2005**, *100*, 801–818. [\[CrossRef\]](#)
10. Singer, D.A. World class base and precious metal deposits—A quantitative analysis. *Econ. Geol.* **1995**, *90*, 88–104. [\[CrossRef\]](#)
11. Jones, B.K. Application of metal zoning to gold exploration in porphyry copper systems. *J. Geochem. Explor.* **1992**, *43*, 127–155. [\[CrossRef\]](#)
12. Presnell, R.D.; Parry, W.T. Geology and geochemistry of the Barney Canyon gold deposit, Utah. *Econ. Geol.* **1996**, *91*, 273–288. [\[CrossRef\]](#)
13. Redmond, P.B.; Einaudi, M.T. The Bingham Canyon porphyry Cu-Mo-Au deposit. I. Sequence of intrusions, vein formation, and sulfide deposition. *Econ. Geol.* **2010**, *105*, 43–68. [\[CrossRef\]](#)
14. Sillitoe, R.H. A plate tectonic model for the origin of porphyry copper deposits. *Econ. Geol.* **1972**, *67*, 184–197. [\[CrossRef\]](#)
15. Grondahl, C.; Zajacz, Z. Magmatic controls on the genesis of porphyry Cu-Mo-Au deposits: The Bingham Canyon example. *Earth Planet. Sci. Lett.* **2017**, *480*, 53–65. [\[CrossRef\]](#)
16. Waite, K.A.; Keith, J.D.; Christiansen, E.H.; Whitney, J.A.; Hattori, K.; Tingey, D.G.; Hook, C.J. Petrogenesis of the volcanic and intrusive rocks associated with the Bingham Canyon porphyry Cu-Au-Mo deposit, Utah. *Soc. Econ. Geol. Guideb. Ser.* **1997**, *29*, 69–90.
17. Atkinson, W.W., Jr.; Einaudi, M.T. Skarn formation and mineralization in the contact aureole at Carr Fork, Bingham, Utah. *Econ. Geol.* **1978**, *73*, 1326–1365. [\[CrossRef\]](#)

18. Lanier, G.; John, E.C.; Swensen, A.J.; Reid, J.; Bard, C.E.; Caddey, S.W.; Wilson, J.C. General geology of the Bingham Mine, Bingham Canyon, Utah. *Econ. Geol.* **1978**, *73*, 1228–1241. [[CrossRef](#)]
19. Core, D.P.; Kesler, S.E.; Essene, E.J. Unusually Cu-rich magmas associated with giant porphyry copper deposits: Evidence from Bingham, Utah. *Geology* **2006**, *34*, 41–44. [[CrossRef](#)]
20. Zhang, D.; Audétat, A. What caused the formation of the giant Bingham Canyon porphyry Cu-Mo-Au deposit? Insights from melt inclusions and magmatic sulfides. *Econ. Geol.* **2017**, *112*, 221–244. [[CrossRef](#)]
21. Von Quadt, A.; Erni, M.; Martinek, K.; Moll, M.; Peytcheva, I.; Heinrich, C.A. Zircon crystallization and the lifetimes of ore-forming magmatic-hydrothermal systems. *Geology* **2011**, *39*, 731–734. [[CrossRef](#)]
22. Landtwing, M.R.; Furrer, C.; Redmond, P.B.; Pettke, T.; Guillong, M.; Heinrich, C.A. The Bingham Canyon porphyry Cu-Mo-Au deposit. III. Zoned copper-gold ore deposition by magmatic vapor expansion. *Econ. Geol.* **2010**, *105*, 91–118. [[CrossRef](#)]
23. Cunningham, C.G.; Austin, G.W.; Naeser, C.W.; Rye, R.O.; Ballantyne, G.H.; Stamm, R.G.; Barker, C.E. Formation of a paleothermal anomaly and disseminated gold deposits associated with the Bingham Canyon porphyry Cu-Au-Mo system, Utah. *Econ. Geol.* **2004**, *99*, 789–806. [[CrossRef](#)]
24. Cline, J.S.; Hofstra, A.H.; Muntean, J.L.; Tosdal, R.M.; Hickey, K.A. Carlin-type deposits gold deposits in Nevada: Critical geologic characteristics and viable models. *Econ. Geol. 100 Anniv. Vol.* **2005**, *451*, 484.
25. Babcock, R.C., Jr.; Ballantyne, G.H.; Phillips, C.H. Summary of the geology of the Bingham District, Utah. *Ariz. Geol. Soc. Dig.* **1995**, *20*, 316–335.
26. Cunningham, C.G.; Austin, G.W.; Naeser, C.W.; Rye, R.O.; Ballantyne, G.H.; Stamm, R.G.; Barker, C.E. Formation of a paleothermal anomaly and disseminated gold deposits associated with the Bingham Canyon porphyry Cu-Au-Mo system, Utah—A reply. *Econ. Geol.* **2005**, *100*, 594–595. [[CrossRef](#)]
27. Presnell, R.D.; Parry, W.T. Formation of a paleothermal anomaly and disseminated gold deposits associated with the Bingham Canyon porphyry Cu-Au-Mo system, Utah—A discussion. *Econ. Geol.* **2005**, *100*, 591–593. [[CrossRef](#)]
28. McGoldrick, P.J.; Keays, R.R.; Scott, B.B. Thallium: A sensitive indicator of rock/seawater interaction and of sulfur saturation of silicate melts. *Geochim. Cosmochim. Acta* **1979**, *43*, 1301–1311. [[CrossRef](#)]
29. Noll, P.D., Jr.; Newsom, H.E.; Leeman, W.P.; Ryan, J.G. The role of hydrothermal fluids in the production of subduction zone magmas: Evidence from siderophile and chalcophile trace elements and boron. *Geochim. Cosmochim. Acta* **1996**, *60*, 587–611. [[CrossRef](#)]
30. Rehkamper, M.; Nielsen, S.G. The mass balance of dissolved thallium in the oceans. *Mar. Chem.* **2004**, *85*, 125–139. [[CrossRef](#)]
31. Nielsen, S.G.; Rehkamper, M.; Prytulak, J. Investigation and application of thallium isotope fractionation. *Rev. Mineral. Geochem.* **2017**, *82*, 759–798. [[CrossRef](#)]
32. Shaw, D.M. The geochemistry of thallium. *Geochim. Cosmochim. Acta* **1952**, *2*, 118–154. [[CrossRef](#)]
33. Prytulak, J.; Brett, A.; Webb, M.; Plank, T.; Rehkamper, M.; Savage, P.S.; Woodhead, J. Thallium elemental behavior and stable isotope fractionation during magmatic processes. *Chem. Geol.* **2017**, *448*, 71–83. [[CrossRef](#)]
34. Bea, F.; Pereira, M.D.; Stroh, A. Mineral/leucosome trace-element partitioning in a peraluminous migmatite (a laser ablation-ICP-MS study). *Chem. Geol.* **1994**, *117*, 291–312. [[CrossRef](#)]
35. Kiseeva, E.S.; Wood, B.J. A simple model for chalcophile element partitioning between sulphide and silicate liquids with geochemical applications. *Earth Planet. Sci. Lett.* **2013**, *383*, 68–81. [[CrossRef](#)]
36. Rader, S.T.; Mazdab, F.K.; Barton, M.D. Mineralogical thallium geochemistry and isotope variations from igneous, metamorphic, and metasomatic systems. *Geochim. Cosmochim. Acta* **2018**, *243*, 42–65. [[CrossRef](#)]
37. Vink, B.W. The behavior of thallium in the (sub) surface environment in terms of Eh and pH. *Chem. Geol.* **1993**, *109*, 119–123. [[CrossRef](#)]
38. Batley, G.E.; Florence, T.M. Determination of thallium in natural waters by anodic stripping voltammetry. *J. Electroanal. Chem.* **1975**, *61*, 205–211. [[CrossRef](#)]
39. Nielsen, S.G.; Rehkamper, M.; Teagle, D.A.H.; Butterfield, D.A.; Alt, J.C.; Halliday, A.N. Hydrothermal fluid fluxes calculated from the isotopic mass balance of thallium in the ocean crust. *Earth Planet. Sci. Lett.* **2006**, *251*, 120–133. [[CrossRef](#)]
40. Coggon, R.M.; Rehkamper, M.; Atteck, C.; Teagle, D.A.H.; Alt, J.C.; Cooper, M.J. Controls on thallium uptake during hydrothermal alteration of the upper ocean crust. *Geochim. Cosmochim. Acta* **2014**, *144*, 25–42. [[CrossRef](#)]

41. Nielsen, S.G.; Rehkamper, M.; Norman, M.D.; Halliday, A.N.; Harrison, D. Thallium isotopic evidence for ferromanganese sediments in the mantle source of Hawaiian basalts. *Nature* **2006**, *439*, 314–317. [[CrossRef](#)] [[PubMed](#)]
42. Brett, A.; Prytulak, J.; Hammond, S.J.; Rehkamper, M. Thallium mass fraction and stable isotope ratios of sixteen geological reference materials. *Geostand. Geoanal. Res.* **2018**. [[CrossRef](#)]
43. Prytulak, J.; Nielsen, S.G.; Plank, T.; Barker, M.; Elliott, T. Assessing the utility of thallium and thallium isotopes for tracing subduction zone inputs to the Mariana arc. *Chem. Geol.* **2013**, *345*, 139–149. [[CrossRef](#)]
44. Nielsen, S.G.; Yogodzinski, G.; Prytulak, J.; Plank, T.; Kay, S.; Kay, R.; Blusztajn, J.; Owens, J.; Auro, M.; Kading, T. Tracking along-arc sediment inputs to the Aleutian arc using thallium isotopes. *Geochim. Cosmochim. Acta* **2016**, *181*, 217–237. [[CrossRef](#)]
45. Nielsen, S.G.; Prytulak, J.; Blusztajn, J.; Shu, Y.; Auro, M.; Regelous, M.; Walker, J. Thallium isotopes as tracers of recycled materials in subduction zones: Review and new data from Tonga-Kermadec and Central America. *J. Volcanol. Geotherm. Res.* **2017**, *339*, 23–40. [[CrossRef](#)]
46. Shu, Y.; Nielsen, S.G.; Zeng, Z.; Shinjo, R.; Blusztajn, J.; Wang, X.; Chen, S. Tracing subducted sediment inputs to the Ryukyu arc-Okinawa trough system: Evidence from thallium isotopes. *Geochim. Cosmochim. Acta* **2017**, *217*, 462–491. [[CrossRef](#)]
47. Bigeleisen, J.; Mayer, M.G. Calculation of equilibrium constants for isotopic exchange reactions. *J. Chem. Phys.* **1947**, *15*, 261–267. [[CrossRef](#)]
48. Baker, R.G.A.; Rehkamper, M.; Ihlenfeld, C.; Oates, C.J.; Coggon, R. Thallium isotope variations in an ore-bearing continental igneous setting: Collahuasi Formation, northern Chile. *Geochim. Cosmochim. Acta* **2010**, *74*, 4405–4416. [[CrossRef](#)]
49. Munizaga, F.; Makshev, V.; Fanning, C.M.; Giglio, S.; Yaxley, G.; Tassinari, C.C.G. Late Paleozoic–Early Triassic magmatism on the western margin of Gondwana: Collahuasi area, northern Chile. *Gondwana Res.* **2008**, *13*, 407–427. [[CrossRef](#)]
50. Masterman, G.J.; Cooke, D.R.; Berry, R.F.; Clark, A.H.; Archibald, D.A.; Mathur, R.; Walshe, J.L.; Durán, M. $^{40}\text{Ar}/^{39}\text{Ar}$ and Re–Os geochronology of porphyry copper–molybdenum deposits and related copper–silver veins in the Collahuasi district, northern Chile. *Econ. Geol.* **2004**, *99*, 673–690. [[CrossRef](#)]
51. Masterman, G.J.; Cooke, D.R.; Berry, R.F.; Walshe, J.L.; Lee, A.W.; Clark, A.H. Fluid chemistry, structural setting, and emplacement history of the Rosario Cu–Mo porphyry and Cu–Ag–Au epithermal veins, Collahuasi District, northern Chile. *Econ. Geol.* **2005**, *100*, 835–862. [[CrossRef](#)]
52. Rehkamper, M.; Frank, M.; Hein, J.R.; Porcelli, D.; Halliday, A.; Ingri, J.; Liebetrau, V. Thallium isotope variations in seawater and hydrogenetic, diagenetic, and hydrothermal ferromanganese deposits. *Earth Planet. Sci. Lett.* **2002**, *197*, 65–81. [[CrossRef](#)]
53. Rehkamper, M.; Frank, M.; Hein, J.R.; Halliday, A. Cenozoic marine geochemistry of thallium deduced from isotopic studies of ferromanganese crusts and pelagic sediments. *Earth Planet. Sci. Lett.* **2004**, *219*, 77–91. [[CrossRef](#)]
54. Wickham, K. Thallium Isotope Implications for the Metalliferous Source of Carlin-Type Gold Deposits in Northern Nevada. Master’s Thesis, University of Nevada, Reno, NV, USA, 2014.
55. Hettmann, K.; Marks, M.A.W.; Kreissig, K.; Zack, T.; Wenzel, T.; Rehkamper, M.; Jacob, D.E.; Markl, G. The geochemistry of Tl and its isotopes during magmatic and hydrothermal processes: The peralkaline Ilimaussaq complex, southwest Greenland. *Chem. Geol.* **2014**, *366*, 1–13. [[CrossRef](#)]
56. Hettmann, K.; Kreissig, K.; Rehkamper, M.; Wenzel, T.; Mertz-Kraus, R.; Markl, G. Thallium geochemistry in the metamorphic Lengenbach sulfide deposit, Switzerland: Thallium-isotope fractionation in a sulfide melt. *Am. Mineral.* **2014**, *99*, 793–803. [[CrossRef](#)]
57. Peter, J.M.; Gadd, M.G.; Layton-Matthews, D.; Voinot, A. Reconnaissance thallium isotope study of zinc–lead SEDEX mineralization and host rocks in the Howard’s Pass district, Selwyn Basin, Yukon: Potential application to paleoredox determinations and fingerprinting of mineralization. In *Targeted Geoscience Initiative: 2017 Report of Activities*; Rogers, N., Ed.; Geological Survey of Canada: Ottawa, ON, Canada, 2018; Volume 3, Open File 8358; pp. 173–191.
58. Rehkamper, M.; Halliday, A.N. The precise measurement of Tl isotopic compositions by MC-ICPMS: Application to the analysis of geological materials and meteorites. *Geochim. Cosmochim. Acta* **1999**, *63*, 935–944. [[CrossRef](#)]
59. Nielsen, S.G.; Rehkamper, M.; Baker, J.; Halliday, A.N. The precise and accurate determination of thallium isotope compositions and concentrations for water samples by MC-ICPMS. *Chem. Geol.* **2004**, *204*, 109–124. [[CrossRef](#)]

60. Baker, R.G.A.; Rehkamper, M.; Hinkley, T.K.; Nielsen, S.G.; Toutain, J.P. Investigation of thallium fluxes from subaerial volcanism—Implications for the present and past mass balance of thallium in the oceans. *Geochim. Cosmochim. Acta* **2009**, *73*, 6340–6359. [[CrossRef](#)]
61. Rudnick, R.L.; Gao, S. Composition of the continental crust. In *Treatise on Geochemistry*; Rudnick, R.L., Ed.; Elsevier Ltd: Amsterdam, The Netherlands, 2014; Volume 3, p. 659.
62. Parry, W.T.; Jasumback, M.; Wilson, P.N. Clay mineralogy of phyllic and intermediate argillic alteration at Bingham, Utah. *Econ. Geol.* **2002**, *97*, 221–239. [[CrossRef](#)]
63. Cameron, D.E.; Garmoe, W.J. Geology of skarn and high-grade gold in the Carr Fork Mine, Utah. *Econ. Geol.* **1987**, *82*, 1319–1333. [[CrossRef](#)]
64. Xiong, J. Hydrothermal thallium mineralization up to 300 °C: A thermodynamic approach. *Ore Geo. Rev.* **2007**, *32*, 291–313. [[CrossRef](#)]
65. Roedder, E. Fluid inclusion studies on the porphyry-type ore deposits at Bingham, Utah, Butte, Montana, and Climax, Colorado. *Econ. Geol.* **1971**, *66*, 98–118. [[CrossRef](#)]
66. Arehart, G.B. Characteristics and origin of sediment-hosted disseminated gold deposits: A review. *Ore Geo. Rev.* **1996**, *11*, 383–403. [[CrossRef](#)]
67. Arehart, G.B.; Chakurian, A.M.; Tretbar, D.R.; Christensen, J.N.; McInnes, B.A.; Donelick, R.A. Evaluation of radioisotope dating of Carlin-type deposits in the Great Basin, western North America, and implications for deposit genesis. *Econ. Geol.* **2003**, *98*, 235–248. [[CrossRef](#)]



© 2018 by the authors. Licensee MDPI, Basel, Switzerland. This article is an open access article distributed under the terms and conditions of the Creative Commons Attribution (CC BY) license (<http://creativecommons.org/licenses/by/4.0/>).